

***In situ* pressure study of Rb₄C₆₀ insulator to metal transition by Compton scattering**

A. A. Sabouri-Dodaran

*Institute for Studies in Theoretical Physics and Mathematics, Tehran 19395-5531, Iran
and Payame Noor University, Tehran 19395-4697, Iran*

Ch. Bellin and G. Loupiau

*Institut de Minéralogie et Physique des Milieux Condensés, Université Paris VI et VII, URA CNRS 7590, case 115, 4 place Jussieu,
75252 Paris cedex 05, France*

M. Marangolo

*Institut des Nanosciences de Paris, Université Paris VI et VII, URA CNRS 7588, case 115, 4 place Jussieu, 75252 Paris cedex 05,
France*

S. Rabii

Department of Electrical and Systems Engineering, University of Pennsylvania, Philadelphia, Pennsylvania 19104-6390, USA

F. Rachdi

GDPIC, Université Montpellier II, place Eugène Bataillon, F-34095 Montpellier Cedex 05, France

Th. Buslaps and M. Mezouar

European Synchrotron Radiation Facility (ESRF), BP 220, 38043 Grenoble-Cedex, France

(Received 21 December 2004; published 3 August 2005)

Compton scattering has been shown to be a powerful tool for studying the ground state electronic density in real materials. Using synchrotron radiation, we have studied pressure effects on Rb₄C₆₀ by measuring the Compton profiles below and above the insulator to metal transition at 0.8 GPa. The experimental results are compared with the corresponding calculated results, obtained from new *ab initio* energy band structure calculations. These results allow us to quantitatively evaluate contributions to the Compton profiles resulting from the contraction of the unit cell as well as from the contraction of the C₆₀ molecule itself. In this paper, we point out an unexpected contraction of the volume of the C₆₀ molecule, leading to a major effect on the electronic density of the Rb₄C₆₀ compound.

DOI: [10.1103/PhysRevB.72.085412](https://doi.org/10.1103/PhysRevB.72.085412)

PACS number(s): 71.20.Tx, 78.70.Ck, 71.15.Mb, 61.46.+w

I. INTRODUCTION

The family of compounds, A_nC₆₀ (A=K, Rb and Cs; $n=1, 3, 4,$ and 6) exhibits a diversity of structural and electronic properties that has made them the subject of a great deal of interest. They exhibit conductivities ranging from superconducting ($n=3$) to insulating ($n=6$) as a function of the alkali ion concentration.¹ Recall that the neutral C₆₀ molecule possesses a closed shell electronic structure in its ground state. Therefore, within a rigid band picture, the threefold degenerate molecular orbital t_{1u} of the pristine C₆₀ is partially occupied by electrons provided by the alkali atoms, resulting in metallic behaviors for A₃C₆₀ and A₄C₆₀ compounds, whereas the three suborbitals are filled for A₆C₆₀, leading to an insulator. In particular, the unusual behavior of the A₄C₆₀ family has intrigued the fullerene community. To begin with, x-ray powder patterns indicate that their structure is body-centered tetragonal (bct), whereas the other alkali intercalated compounds are all cubic,² except for A₁C₆₀, which is polymerized.³ Furthermore, A₄C₆₀ compounds are nonmagnetic insulators at ambient pressure, as evidenced by NMR⁴ and photoemission⁵ experiments. A possible explanation of this behavior is provided by Fabrizio and Tosatti,^{6,7} postulating a strong Coulomb repulsion that drives

the system into a Mott insulator phase. This is accompanied by a Jahn-Teller splitting that overcomes the Hund rule, making the insulator nonmagnetic. The Jahn-Teller distortion removes the degeneracy of the threefold t_{1u} , leading to two lower suborbitals separated from the upper one.^{7,8} In A₄C₆₀ the four electrons given by the alkali atoms fill the lower set, leading to an insulator behavior.

Furthermore, A₄C₆₀ compounds undergo an insulator to metal transition under pressure around 0.8 GPa, observed by the NMR study of Rb₄C₆₀,⁹ performed under pressure up to 12 kbar. Surprisingly, this observation did not lead to further investigation until our diffraction experiment, which exhibits an abrupt jump in the compressibility between 0.5 and 0.8 GPa. We attributed this jump to a structural phase transition preserving the tetragonal symmetry.¹⁰ In the present study, we go beyond the determination of the equation of states and focus on the study of the electronic density modification produced under pressure. Thus we have performed simultaneous Compton scattering and diffraction experiments, at pressures below and above the insulator-metal transition (i.e., 0.2 and 2 GPa). This enabled us to follow the electronic density change in momentum space caused by this phase transition. The wave functions obtained from *ab initio* energy band calculations of Rb₄C₆₀ were used to calculate Compton profiles be-

low and above the transition. Compton scattering is a bulk probe and, due to its incoherence, it is not sensitive to defects in the sample. Therefore it is particularly suitable for the investigation of synthetic materials. Furthermore, it is specially sensitive to delocalized states in the solid, i.e., valence and conduction electrons. We have already demonstrated the utility of this approach in the case of intercalated fullerenes.^{11–13} Since the information provided by Compton scattering about the ground-state electron distribution can be directly related to the Fourier expansion of the wave functions, it provides an excellent direct probe of the quality of calculated wave functions. Conversely, the calculated are used to understand and quantify the different electronic contributions to the Compton profile. These include the possible roles played by the C₆₀ molecular distortion, the contractions unit-cell volume and that of the C₆₀ molecular volume with pressure. The latter has been heretofore assumed to be negligible.

In Secs. II and III we present the Compton scattering method and the theoretical approach. In Sec. IV we describe the experimental procedures, including the sample preparation and characterization. The results are presented, discussed, and followed by concluding remarks in Sec. V.

II. COMPTON SCATTERING METHOD

Compton scattering involves the inelastic scattering of photons by electrons. The conservations of energy and momentum lead to a relationship between the energy loss of the photon and the projection of the initial electron momentum along the scattering vector \mathbf{K} . The component of this energy loss resulting from scattering by the electrons at rest is referred to as the Compton shift. In addition, the motion of the electrons in the system results in a Doppler broadening of the distribution around the Compton shift and is a direct indicator of their initial momentum distribution.

In the impulse approximation (IA), that inelastic scattering process is assumed to be fast enough for the interaction potential to remain unchanged. Within this approximation, the Compton profile is defined as

$$J(q, \mathbf{e}) = \int n(\mathbf{p}) \delta(\mathbf{p} \cdot \mathbf{e} - q) d\mathbf{p} = \int \chi^*(\mathbf{p}) \chi(\mathbf{p}) \delta(\mathbf{p} \cdot \mathbf{e} - q) d\mathbf{p}, \quad (1)$$

where \mathbf{e} is the unit vector along the scattering vector \mathbf{K} , $n(\mathbf{p})$ the electron momentum density, and $\chi(\mathbf{p})$ the electron wave function in momentum space, i.e., Fourier transform of the wave function in real space.^{14–16} Throughout the remainder of this paper we shall use atomic units (a.u.), for which $\hbar = m = 1$.

III. THEORETICAL APPROACH

The electronic structure of Rb₄C₆₀ was calculated first using the standard atomic positions, as determined by x-ray diffraction and, second, using those obtained by geometrical optimization.¹⁷ We employ the density functional theory in the local density approximation and using norm-conserving

pseudopotentials.¹⁸ For carbon atoms, we use $2s$ and $2p$ as valence states. For rubidium atoms, we assumed an ionized configuration $4s^2 4p^6 4d^0$, treating $4s$, $4p$, and $4d$ as valence states. The wave functions were expanded in plane waves using a 60 Ry Cutoff. We used a $2 \times 2 \times 2$ Monkhorst-Pack grid¹⁹ (four inequivalents \mathbf{k} points) for the electronic Brillouin zone (BZ) integration and a Gaussian smearing of 0.2 eV. The calculations were self-consistent, with no restriction on the form of charge density or potential. Due to the large size of the unit cell, four \mathbf{k} points were sufficient to achieve convergence in the BZ integration.

The calculated ground-state wave functions are represented by their plane wave expansion,

$$\psi_{n,\mathbf{k}}(\mathbf{r}) = \sum_{\mathbf{G}} C_{n,\mathbf{k}}(\mathbf{G}) \exp[i(\mathbf{k} + \mathbf{G}) \cdot \mathbf{r}], \quad (2)$$

where \mathbf{G} 's are reciprocal lattice vectors. The large size of the primitive unit cell for this compound results in very short lengths of the reciprocal lattice vectors. Therefore the number of \mathbf{G} 's necessary to obtain convergence in this sum is as large as 40.000. Using this expansion, Eq. ((2)) for the directional Compton profile takes the following form:

$$J(q, \mathbf{e}) = \frac{1}{N} \sum_n \sum_{\mathbf{k}} \sum_{\mathbf{G}} |C_{n,\mathbf{k}}(\mathbf{G})|^2 \delta((\mathbf{k} + \mathbf{G}) \cdot \mathbf{e} - q) \vartheta(E_n - E_f). \quad (3)$$

The summation \mathbf{G} is over all the reciprocal lattice vectors for which the $C_{n,\mathbf{k}}(\mathbf{G})$'s are non-negligible. The summation \mathbf{k} is over the symmetry-reduced sector of the BZ of the Rb₄C₆₀ compound is carried out using a tetrahedral interpolation method.²⁰ The volume of this irreducible sector of the BZ is divided into tetrahedra by choosing a grid of \mathbf{k} points. The actual wave functions are calculated at each grid point and a linear interpolation is carried out for $|C_{n,\mathbf{k}}(\mathbf{G})|^2$ within each tetrahedron. Due to the small size of the BZ for these compounds, a relatively coarse mesh of 13 points was sufficient for the BZ integration. The summation n is over the occupied states. The function ϑ cuts off this summation at the Fermi energy in the case of a metal or a semi metal. Since the measurements are performed on powder samples, the comparison with experiment is made with an average theoretical profile obtained from four calculated directional profiles, i.e., (0 0 1), (0 1 0), (1 0 0), (1 1 *a/c*).

Our calculations were performed for a rigid configuration fixing the C₆₀ molecules in the most symmetric configuration,¹ i.e., with the three double bonds chosen perpendicular to $\langle 100 \rangle$ directions and with the $\langle 111 \rangle$ directions passing through centers of hexagons.¹⁰ However, in a previous paper,¹¹ we reported the difference between Compton profiles of C₆₀ powder at temperatures below and above the orientational ordering phase transition (260 K). We showed that this difference was not larger than the statistical error. As a consequence, the average Compton profile resulting from the measurement on a powder sample is not sensitive to the orientational disorder of the C₆₀ molecule.

IV. EXPERIMENTAL PROCEDURE

We used a sample coming from the same origin as those used in the NMR measurement that exhibited the insulator-metal transition.⁹ The Rb₄C₆₀ sample was prepared from a C₆₀ powder. After rubidium doping up to saturation to form Rb₆C₆₀, Rb₄C₆₀ was obtained by reacting stoichiometric amounts of Rb₆C₆₀ and C₆₀, as described in Ref. 21.

The experiments were carried out using the high-energy beamline (Insertion Device 15B) of the European Synchrotron Radiation Facility in Grenoble, France.²² The synchrotron radiation beam was monochromatized to select 55.8 keV photons that were focused on a powder sample kept inside the pressure cell. This energy was chosen in order to optimize the positions of the Raman departures due to rubidium atoms with respect to the Compton peak position, i.e., to shift them as far as possible from the Compton peak. Rb1s leads to a Raman departure at 9.4 a.u. (the low-energy side of the profile) and Rb2s leads to a Raman departure at -11 a.u. (the high-energy side). We used a large volume apparatus (Paris-Edinburgh cell²³) as the pressure cell for combined diffraction and Compton measurements at pressures below and above the insulator-metal transition, i.e., at 0.2 GPa and 2 GPa, respectively.

The simultaneous diffraction measurements were performed for two different purposes: (i) to monitor cell parameters and sample symmetry; and (ii) to deduce the value of the pressure from the already known boron nitride equation of state (used as a pressure calibration standard).²⁴ Diffraction patterns were collected in an angle-resolved geometry on an image-plate detector (MAR345). By moving the pressure cell perpendicular to the x-ray beam, we were able to obtain the spectra from the sample, the internal pressure calibrant (hexagonal boron nitride—hBN), and the sample environment (boron epoxy and hBN) successively. The two-dimensional diffraction images were analyzed using the ESRF Fit2D software, yielding intensity vs 2θ patterns.

Compton scattering spectra were measured using a germanium detector under a scattering angle of 160 deg. In order to avoid all signals coming from the sample environment, a set of slits have been carefully designed, mounted before and after the sample, and checked in order to confine the scattering lozenge totally within the sample. The resolution function is deduced from the full width at half-maximum (FWHM) of the thermal diffuse scattering (TDS) peak and is equal to 0.46 a.u. After subtracting the background and correcting profiles from the energy dependent contributions (absorption in air, sample, and anvil cell, as well as detector efficiency), the wavelength scale was converted into momentum scale. Multiple elastic and inelastic scattering contributions (MSC) for each measured profile have been calculated using a Monte Carlo simulation, taking into account beam polarization, sample geometry, and density.²⁵ MSC was then subtracted from measured profiles. Both measured spectra were normalized to the compound's full number of electrons per carbon atom between -9.5 and 9.5 a.u., i.e., 8.13 electrons. Since many of the systematic errors cancel when one takes the difference between low- and high-pressure Compton measurements, the results are presented in the form of the difference between the two profiles.

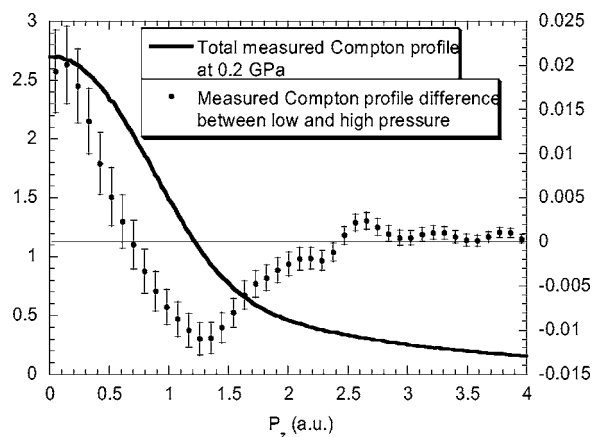


FIG. 1. Total measured Compton profile at low pressure (left scale) and the difference between low- and high-pressure measured Compton profiles (right scale).

V. RESULTS AND DISCUSSION

A. Experimental results

In Fig. 1, we show the measured Compton profile difference (CP difference), defined as the Compton profile measured at low pressure minus the Compton profile measured at high pressure. Five points are shown in the resolution range of 0.46 a.u., Here 9×10^5 and 2×10^5 counts have been integrated in a of 0.1 a.u. range at the top of the Compton profile for the low- and the high-pressure spectra respectively. Statistical error bars were calculated within a range of 0.1 a.u. The measured CP difference is symmetric up to 9.5 a.u., within the statistical accuracy of the experiment. As a consequence, the CP difference is symmetrized, leading to a reduction of the statistical error bars by a factor of $\sqrt{2}$.

Two main features on the CP difference should be pointed out. The maximum magnitude occurs at $p_z=0$ a.u. and reaches 1% of the total profile, and the minimum is located around $p_z=1.3$ a.u.

The following discussion will concentrate on the description of these two features by comparing them with the *ab initio* calculations. The figure also gives the total profile at 0.2 GPa.

The high- and low-pressure cell parameters needed for the calculations are obtained from a detailed analysis of our x-ray diffraction 2θ patterns. Our low-pressure cell parameters are in perfect agreement with previous measurements,² i.e., $a=11.96$ Å and $c=11.02$ Å. At high pressure we obtain $a=11.82$ Å and $c=10.63$ Å,¹⁰ recalling that there is no structural change of symmetry under pressure.

We can rule out the possible polymerization, i.e., the breaking of double bonds through the formation of rings joining two C₆₀ molecules, for the following two reasons. First, the diffraction patterns obtained¹⁰ do not show any evidence of polymerization between C₆₀ molecules up to 5 GPa in contrast to that reported for C₆₀.²⁶ Second, if we compare the distance between the adjacent C₆₀ molecules in Rb₄C₆₀ and the polymerized compounds such as Li₄C₆₀ or Na₄C₆₀, we can conclude that Rb₄C₆₀ is not polymerized in the pressure range used in this study. A simple geometrical

consideration provides C_{60} molecule center-to-center distances in Rb_4C_{60} equal to 10.09 Å at ambient pressure and 9.90 Å at 2 GPa. In contrast, the corresponding values are 9.13 Å and 9.28 Å for Li_4C_{60} (double bonding monomers²⁷) and Na_4C_{60} (singly bonded monomers²⁸), respectively. As a consequence, if we consider a diameter of C_{60} molecule close to 7.1 Å,² the C–C bond length between two adjacent molecules becomes equal to 2.80 Å for Rb_4C_{60} at high pressure (2 GPa), 2.18 Å for Na_4C_{60} , and 2.03 Å for Li_4C_{60} . Third, C–C bond length values between 1.7 to 1.9 Å^{29,30} are observed in other polymers formed by 2+2 cycloaddition such as RBC_{60} .²⁹ Such values, which are also the highest possible values predicted by DFT in polymeric fullerenes,³¹ are much lower than for Rb_4C_{60} . As a consequence, we infer that the C–C bond length in Rb_4C_{60} is too large to indicate that the cycloaddition process occurs, at least up to 2 GPa. Furthermore, if the C_{60} molecule contracts under pressure, the C–C bond length between two adjacent molecules would become larger than 2.80 Å, making the polymerization even more unlikely.

B. Discussion

Three different components may contribute to the Compton profile difference.

(i) The so-called Jahn-Teller distortion, i.e., distortion of the C_{60} molecule at ambient pressure. This distortion is assumed to be modified under pressure. It should be noted that this phenomenon has never been experimentally clearly observed, even if its role in driving A_4C_{60} into an insulating phase is widely accepted.

(ii) The unit cell contraction under pressure, i.e., a decrease of cell-parameter values as measured by our diffraction experiments.

(iii) The volume contraction of the C_{60} molecule under pressure.

In order to better understand the difference profile between low- and high-pressure measurements, we will present the effect of each of the three contributions listed above obtained by means of our LDA calculations.

1. Distortion of the C_{60} molecule

a. Isolated C_{60} molecule. We study the effect of the distortion of the C_{60} “ball” resulting from the transfer of electrons from alkali atoms to the C_{60} molecule. We define the diameter of the C_{60} ball as the distance separating two carbon atoms symmetrically set on opposite sides of the molecule center. In the three cases below, we used the tight binding method³² to generate relaxed positions of carbon atoms in an isolated C_{60} molecule for different models of charge transfer.

(i) Neutral C_{60} molecule. The t_{1u} orbital is empty and the C_{60} molecule remains spherically symmetric after relaxation. This case is hereafter referred to as the “neutral molecule” or “NM.”

(ii) C_{60}^{4-} ion with nonuniform charge distribution. The first two levels of the unoccupied t_{1u} are filled by the four electrons. Therefore occupation numbers of the two lower levels are 2 whereas it is 0 for the upper level. This removal

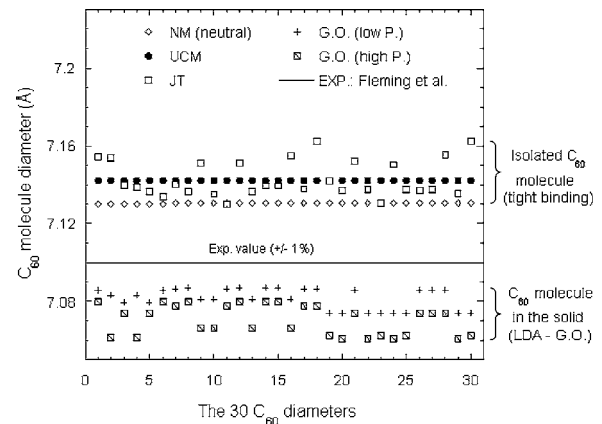


FIG. 2. The 30 diameters of the C_{60} molecule for the following four cases: (i) JT, Jahn-Teller distortion, i.e., relaxation of the four electrons, nonuniformly charged molecule; (ii) UCM, relaxation of the four electrons, uniformly charged molecule (spherical symmetry); (iii) NM, relaxation of the neutral molecule (spherical symmetry); (iv) GO(low P) and GO(high P), C_{60} molecule diameters values obtained with geometrical optimization using LDA calculation performed for the solid Rb_4C_{60} at low and high pressures, respectively.

of degeneracy leads to the Jahn-Teller distortion of the C_{60} hereafter referred to as “JT.”

(iii) C_{60}^{4-} ion with uniform charge distribution. Each of the three suborbitals of t_{1u} is equally filled by the four electrons. Therefore the occupation number of each sublevel is 2/3. As a consequence, there is no distortion of the C_{60} molecule, but only lengthening of all the C–C bonds accompanied by a uniform increase of its volume compared to neutral C_{60} . This case is referred to as the “uniformly charged molecule,” or “UCM,” in the following.

Figure 2 shows the values for the diameter of the C_{60} molecule, as calculated for the three above cases. The result obtained in the UCM case, i.e., 7.14 Å, is in perfect agreement with the previously calculated results obtained by Erwin and Bruder.³³ The molecular distortion in the JT case leads to a dispersion of diameters between 7.13 and 7.16 Å. However, the average value of the JT diameters is very close to that of the UCM.

In order to determine the role played by the distortion of the isolated C_{60} molecule in determining the features of the CP difference, we calculate Compton profiles for both JT and UCM cases. The carbon positions used were obtained from the JT and UCM cases, leading to calculated profiles $J_{JT}(p_z)$ and $J_{UCM}(p_z)$, respectively. In both cases we use rubidium atomic positions² used by Erwin and Bruder,³³ which we will refer to as standard positions in the following discussions.

Thus, the Compton profiles difference $J_{JT}(p_z) - J_{UCM}(p_z)$, shown in Fig. 3, indicates the Jahn-Teller distortion. Its magnitude is negligible [0.01 % of $J(0)$] compared to the experimental CP difference [1% of $J(0)$]. In addition, one can notice that its features are out of phase with the experimental results (Fig. 1). In fact, our calculations have shown that Jahn-Teller distortion affects only individual diameters within C_{60} molecule but not molecular volume itself. There-

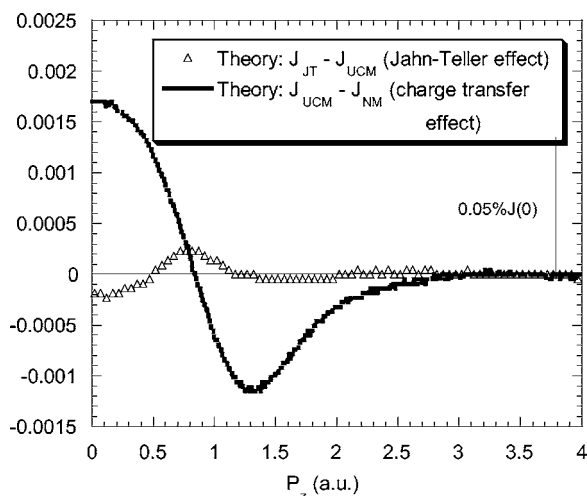


FIG. 3. The Compton profiles (CP) difference between (i) the Jahn-Teller distorted CP, $J_{JT}(p_z)$, and the CP without the Jahn-Teller effect, $J_{UCM}(p_z)$. (ii) The CP without the Jahn-Teller effect, $J_{UCM}(p_z)$, and CP obtained with a neutral C_{60} molecule, $J_{NM}(p_z)$. All calculations were performed using cell-parameter values given by our diffraction results at ambient pressure: $a=11.98 \text{ \AA}$ and $c=11.02 \text{ \AA}$.

fore, we can conclude that such a deformation, with a constant C_{60} molecular volume, has a negligible effect on the CP difference.

In addition, in order to show the charge transfer effect on C_{60} molecules, a second CP difference is shown in Fig. 3, i.e., $J_{UCM}(p_z) - J_{NM}(p_z)$, corresponding to the volume effect in an isotropic C_{60} molecule geometry. $J_{NM}(p_z)$ was also constructed using standard rubidium atomic positions. The electronic charge transfer results in a rather small change of the volume of C_{60} molecule, 0.42%, defined as $[(V_{UCM} - V_{RM})/V_{UCM}] \times 100$. Its contribution to the shape of the CP difference results in a minimum at 1.3 a.u., and by the normalization rule of CP, in a maximum at 0 a.u. Positions of these features are consistent with the experimental CP difference shown in Fig. 1.

Therefore, we conclude that Jahn-Teller distortion is not measurable by the Compton scattering method, but the Compton scattering profile is sensitive to an even smaller change in C_{60} molecular volume.

b. Embedded C_{60} molecule. The C_{60} molecule (hereafter charged C_{60}^{4-}) is placed within the solid Rb_4C_{60} environment, both at low and high pressures. Geometrical optimization was carried out within pseudopotential-LDA formalism to find new positions of carbon and rubidium atoms. Unit-cell parameters were chosen from our diffraction measurements at low as well as at high pressure. These two cases are referred to “geometrically optimized at low pressure,” i.e., “GO(LP)” and “geometrically optimized at high pressure,” i.e., “GO(HP),” respectively. Figure 2 shows the values of the diameter for the embedded C_{60} molecule. They are lower than those corresponding to the isolated molecule, and show a dispersion of 0.015 \AA at low pressure and 0.02 \AA at high pressure. Looking at low-pressure results, we notice that our

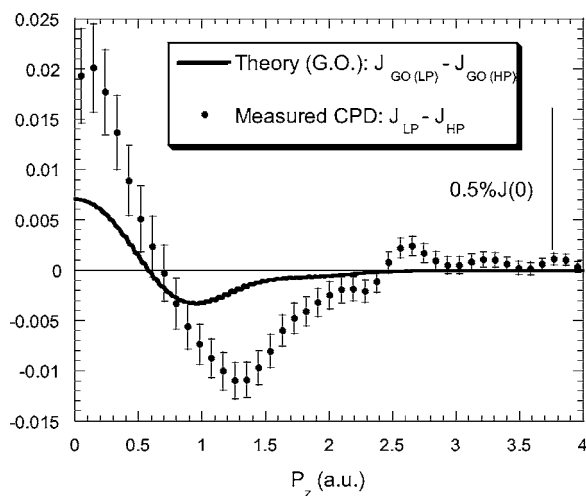


FIG. 4. A comparison between the calculated CP difference performed with geometrical optimization (unit-cell parameters set at experimental values) and the experimental CP difference between low and high pressure.

calculations show that the C_{60} ball is two times less distorted in the case of solid Rb_4C_{60} (GO) than in the isolated case (JT).

In Fig. 4 we show the effect of pressure on the shape of Compton profile difference between low and high pressure, using geometrically optimized LDA calculations. We compare the calculated CP difference $J_{GO(LP)} - J_{GO(HP)}$, with the corresponding experimental result. We observe that the theoretical results do not match the experiment either in amplitude or in position of the measured minimum at $p_z=1.3 \text{ a.u.}$

Figure 2 shows the calculated values for C_{60} diameters for both the isolated molecule as well as for the molecule embedded in the solid. We observe that the average values of the diameters for the GO molecules (for low as well as high pressure) are smaller by about 0.06 \AA than those obtained for the isolated molecule. Kuntscher *et al.* showed by x-ray diffraction that the difference between the C_{60} molecule equatorial radius and the polar radius (along the c axis) is less than 0.08 \AA .³⁴ The average value of 7.12 \AA measured by them is close to the value of 7.10 \AA obtained by Fleming *et al.*,² with an experimental accuracy to within 0.1 \AA . We can therefore conclude that our calculated diameters as well as calculated dispersion values are compatible with experimental results, regardless of the surroundings, i.e., for an isolated C_{60} molecule (neutral or charged) as well as C_{60} surrounded by its solid environment.

2. Cell contraction under pressure

In this section, we follow the shape of the Compton profile as the Rb_4C_{60} unit-cell volume decreases with pressure. Our aim is to evaluate the role of the cell-parameter contraction alone. For this purpose, we assume the C_{60} molecule to be incompressible. Thus, we use the 60 carbon atom positions of the C_{60} molecule as given for UCM in both low- and high-pressure calculations. The relative positions of ru-

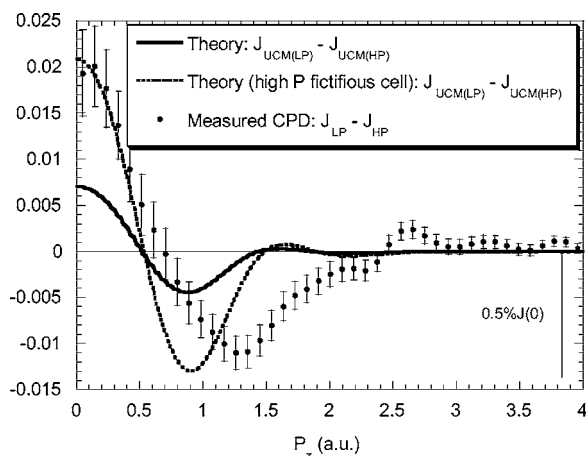


FIG. 5. A comparison between (i) the LDA calculations performed with unit-cell parameters values determined by our x-ray diffraction measurements (and no deformation of the C_{60} molecule under pressure); (ii) the LDA calculations performed with fictitious unit cell parameters values at high pressure; and (iii) the measured CP difference.

bidium atoms in the cell are still standard positions determined by x-ray diffraction,² and do not undergo any varying with pressure. As a result, the only change between low- and high-pressure calculations is the Rb_4C_{60} volume, i.e., the values of the measured cell parameters. Since the C_{60} molecular volume is kept fixed, rubidium atoms become closer to carbon atoms than they are with the C_{60} molecular volume free to decrease with pressure (the actual case). The corresponding CPs will be referred to as $J_{UCM(LP)}$ for low-pressure CP and $J_{UCM(HP)}$ for high-pressure CP.

Figure 5 shows the experimental CP difference between low and high pressure, i.e., $J_{UCM(LP)} - J_{UCM(HP)}$, together with the corresponding calculated CP difference. The calculated result primarily demonstrates the role of the kinetic energy imparted to the unit cell by the application of pressure, leading to a broadening of the CP under pressure.

The experimental and the calculated CP differences show a similar global shape but also clear disagreements. At $p_z = 0$ a.u., the amplitude of the experimental CP difference is higher than the calculated values by a factor 2.8. In addition, the position of the minimum for the experimental CP difference is located at 1.3 a.u., in contrast to 0.85 a.u. for the calculated result.

Going further, we attempted to find whether it was possible to obtain a better agreement between theory and experiment simply by using fictitious cell parameters corresponding to a higher pressure. Fitting the theoretical and the experimental CP difference at $p_z = 0$ a.u. corresponds to an experimental pressure as high as 9 GPa (i.e., $a = 11.55$ Å and $c = 10.30$ Å (Ref. 10)). The calculated difference, using these parameters, is shown in Fig. 5. We can see that the agreement between theory and experiment in the region around $p_z = 1.3$ a.u. is not significantly improved.

3. C_{60} molecular volume in the solid

In this section, we demonstrate the importance of C_{60} molecular volume variation for the shape of the calculated CP

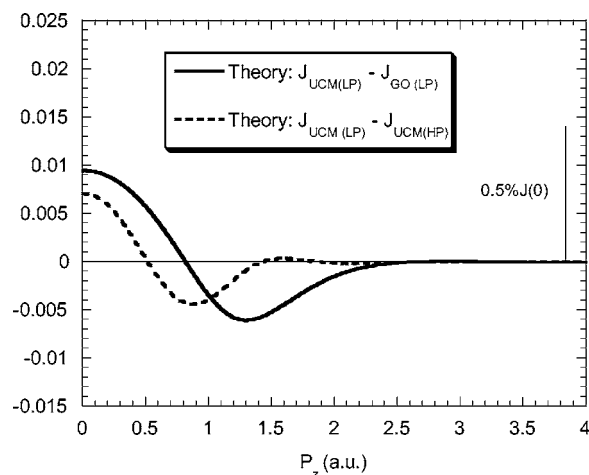


FIG. 6. A comparison between (i) the LDA calculations performed with unit-cell parameters measured by x-ray diffraction (and no deformation of the C_{60} molecule under pressure); and (ii) the difference between the CP calculated for the UCM at low pressure and the CP calculated using geometrical optimization at low pressure.

difference. We focus on what will happen to CP, hypothetically, if we keep both the pressure and Rb_4C_{60} unit-cell volume fixed, allowing only the change of the C_{60} molecular volume. In the following, we chose the fixed pressure to correspond to the low-pressure value.

Therefore, taking as a reference profile UCM(LP) calculations,^{33,6} we used a lower C_{60} molecular volume for the new UCM(LP) calculation than that corresponding to the reference profile. As an example, we chose the GO(LP) calculated diameter (7.14 Å) for the lower volume, a decrease of 0.06 Å (see Fig. 2). This value remains clearly within diffraction experimental accuracy, i.e., 0.1 Å (around 7.10 Å).

The question is, how does this decrease of the molecular volume modify the shape of the Compton profile?

For this purpose, we take the difference between two calculated Compton profiles. First, using the 60 carbon atomic positions given in UCM with the standard Rb atomic positions^{2,33} and denoted as UCM(LP). Second, the profile GO(LP), obtained from the low-pressure LDA calculations with geometrical optimization (the relaxation of Rb and C atomic positions). This is shown in Fig. 6 as $J_{UCM(LP)} - J_{GO(LP)}$ and simply indicates the effect of the C_{60} molecular volume contraction from a diameter corresponding to UCM to that of GO. In order to compare this effect with the so-called cell effect, the CP difference $J_{UCM(LP)} - J_{UCM(HP)}$ is also shown in the same figure.

We notice that the contraction of the C_{60} molecular diameter results in a shift of the minimum of CP difference to the experimental value of $p_z = 1.3$ a.u., and it also leads to an increase of the CP difference at $p_z = 0$ a.u.

C. Final results and concluding remarks

We notice that none of the UCM or GO models are able to describe the experimental CP change under pressure and that

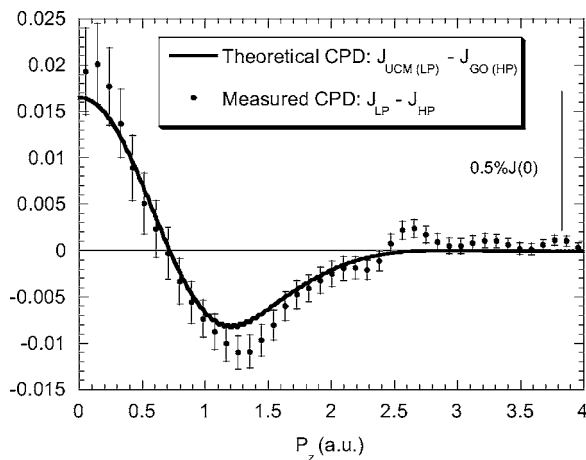


FIG. 7. A comparison between (i) the difference between the CP calculated for the UCM at low pressure and the CP calculated using geometrical optimization at high pressure; and (ii) the measured CP difference.

both give very similar results for the CP difference. In addition, we have already noticed (Sec. I) that Jahn-Teller distortion has a negligible effect on the CP difference. As a consequence, two main contributions have to be taken into account in order to explain the experimental results: (i) C₆₀ molecular volume contraction under pressure and (ii) cell contraction under pressure, i.e., the decrease of cell parameters measured by our diffraction experiments and discussed in Sec. V B 2.

We have seen that the so-called cell contraction effect does not significantly improve the agreement between experiment and theory (fictitious cell—Sec. V B 2). On the other hand, we have pointed out in Sec. V B 3 that the C₆₀ molecular volume effect plays a significant role on the CP difference shape. As a consequence, in order to improve the description of the experimental CP difference when pressure is applied, we have to take into account, not only the effect of pressure on the cell (as given by the difference $J_{GO(LP)} - J_{GO(HP)}$) but also what we infer to be a more realistic molecular volume (as provided by $J_{UCM(LP)} - J_{GO(LP)}$). The addition of these two contributions results in the difference $J_{UCM(LP)} - J_{GO(HP)}$. In Fig. 7, we compare this calculated difference to the experimental CP difference between low and high pressure. We obtain a very good agreement: both the theoretical magnitude at $p_z=0$ a.u. and minimum at $p_z=1.3$ a.u. fit experimental results demonstrating the role played by the C₆₀ molecular volume.

In the present comparison, we consider an average diameter of 7.14 Å for a C₆₀ charged molecule at low pressure (UCM), whereas we consider an average diameter of 7.07 Å at high pressure (GO), leading to a diameter contraction of 0.07 Å under pressure. This 1% diameter contraction corresponds to a 3% contraction of the C₆₀ molecular volume. This volume variation is unexpected since the C₆₀ molecule is usually considered as incompressible. Nevertheless, our

proposed value remains within experimental accuracy of 0.1 Å given by x-ray diffraction experiments.

Within a purely qualitative description, the high-pressure Compton profile is lower and larger around $p_z=0$ a.u. than at low pressure. This is due to a global higher localization under pressure (delocalization in momentum space) of the electrons responsible for the bonding in Rb₄C₆₀. We note that the amplitude at $p_z=0$ a.u. is clearly underestimated by each of the GO and UCM models. In addition, they are not able to reproduce the minimum position at $p_z=1.3$ a.u. We were able to obtain a good description of all features by taking into account a larger decrease of the C₆₀ molecule volume than given by any of these two models.

In conclusion, the shape of the Compton profile difference given by our measurements comes from both of the following:

(i) the contraction of the unit-cell due to pressure, contributing around 35% to the magnitude of the PC difference at $p_z=0$ a.u.

(ii) the contraction of the C₆₀ molecule under pressure that plays a role both on the magnitude (65%) and position of the minimum.

The magnitude of the experimental Compton profile difference between low and high pressure cannot be explained without taking into account a contraction of the C₆₀ molecular volume under pressure. We have shown that a diameter contraction as large as 0.07 Å was required to reproduce the Compton profile difference. The high sensitivity of Compton scattering to the chemical bonding allows the detection of tiny variations of electronic momentum density related to contractions of the C₆₀ molecule diameter. This contraction cannot be seen by the present x-ray diffractions. In a previous paper, we demonstrated, through x-ray diffraction measurements as well as LDA calculations, that the insulator to metal transition is accompanied by an isostructural transition that also leads to an abrupt overall centering of rubidium atoms above C₆₀ molecule pentagons and hexagons.¹⁰ The Compton scattering experiment presented here provides the additional and significant indication of a C₆₀ volume contraction in the pressure range corresponding to an electronic transition. This last conclusion is based on the sensitivity of the Compton scattering to the outer electrons, i.e., electrons responsible for the bonding and subject to charge transfer. The significant change of C₆₀ volume that seems to occur reflects a change in electronic density, resulting in stronger intramolecular bonds than usually predicted.

ACKNOWLEDGMENTS

We are pleased to thank Véronique Brouet, Matteo Calandra, Malcolm Cooper, Francesco Mauri, Abhay Shukla, and Erio Tosatti, for enlightening discussions. We also thank Harald Mueller at ESRF for his very kind and useful help. “*Institut du Développement et des ressources en Informatique Scientifique*” (IDRIS-France) is gratefully acknowledged for calculations performed on the IBM computer (Project No. 021501).

- ¹S. C. Erwin, in *Buckminsterfullerenes*, edited by W. E. Billups and M. A. Ciufolini (VCH, New York, 1993), p. 217; P. J. Benning, J. L. Martins, J. H. Weaver, L. P. F. Chibante, R. E. Smalley, *Science* **252**, 1418 (1991).
- ²R. M. Fleming, M. J. Rosseinsky, A. P. Ramirez, D. W. Murphy, J. C. Tully, R. C. Haddon, T. Siegrist, R. Tycko, S. H. Glarum, P. Marsh, G. Dabbagh, S. M. Zahurak, A. V. Makhija, and C. Hampton, *Nature (London)* **352**, 701 (1991).
- ³O. Chauvet, G. Oszlány, L. Forro, P. W. Stephens, M. Tegze, G. Faigel, and A. Jánossy, *Phys. Rev. Lett.* **72**, 2721 (1994).
- ⁴G. Zimmer, M. Elme, M. Mehring, and F. Rachdi, *Phys. Rev. B* **52**, 13300 (1995).
- ⁵R. Hesper, L. H. Tjeng, A. Heeres, and G. A. Sawatzky, *Phys. Rev. B* **62**, 16046 (2000).
- ⁶M. Fabrizio and E. Tosatti, *Phys. Rev. B* **55**, 13465 (1997).
- ⁷M. Capone, M. Fabrizio, P. Giannozzi, and E. Tosatti, *Phys. Rev. B* **66**, 155123 (2000).
- ⁸J. E. Han, E. Koch, and O. Gunnarson, *Phys. Rev. Lett.* **84**, 1276 (2000); O. Gunnarson, M. Knupfer and J. Fink, *ibid.* **79**, 2714 (1997).
- ⁹R. Kerkoud, P. Auban-Senzier, D. Jérôme, S. Brazovskii, I. Luk'Yanchuk, N. Kirova, F. Rachdi, and C. Goze, *J. Phys. Chem. Solids* **57**, 143 (1996).
- ¹⁰A. A Sabouri-Dodaran, M. Marangolo, Ch. Bellin, F. Mauri, G. Fiquet, G. Loupías, M. Mezouar, W. Crichton, C. Hérold, F. Rachdi, and S. Rabii, *Phys. Rev. B* **70**, 174114 (2004).
- ¹¹J. Moscovici, G. Loupías, S. Rabii, S. Erwin, A. Rassat, and C. Fabre, *Europhys. Lett.* **31**, 87 (1995).
- ¹²M. Marangolo, Ch. Bellin, G. Loupías, S. Rabii, S. Erwin, and T. Buslaps, *Phys. Rev. B* **60**, 17084 (1999).
- ¹³M. Marangolo, J. Moscovici, G. Loupías, S. Rabii, S. Erwin, C. Hérold, J. F. Marêché, and Ph. Lagrange, *Phys. Rev. B* **58**, 7593 (1998).
- ¹⁴P. Eisenberger and P. M. Platzman, *Phys. Rev. A* **2**, 415 (1970).
- ¹⁵M. J. Cooper, *Rep. Prog. Phys.* **48**, 415 (1985).
- ¹⁶M. J. Cooper, P. E. Mijnarends, N. Shiotani, N. Sakai, and A. Bansil, *X-ray Compton scattering*, Oxford Series on Synchrotron Radiation (Oxford Science Publications, New York, 2004).
- ¹⁷Parallel Total Energy Code (PARATEC), <http://www.nersc.gov/projects/paratec/>.
- ¹⁸N. Troullier and J. L. Martins, *Phys. Rev. B* **43**, 1993 (1991).
- ¹⁹H. J. Monkhorst and J. D. Pack, *Phys. Rev. B* **13**, 5188 (1976).
- ²⁰G. Lehmann and M. Taut, *Phys. Status Solidi B* **87**, 221 (1978).
- ²¹J. Reichenbach, F. Rachdi, I. Luk'Yanchuk, M. Ribet, G. Zimmer, and M. Mehring, *J. Chem. Phys.* **101**, 4585 (1994).
- ²²P. Suortti, T. Buslaps, P. Fajardo, V. Honkimäki, M. Kretzschmer, U. Lienert, J. E. McCarthy, M. Renier, A. Shukla, Th. Tschentscher, and T. Meinnander, *J. Synchrotron Radiat.* **6**, 69 (1999).
- ²³J. M. Besson, G. Hamel, T. Grima, R. J. Nelmes, J. S. Loveday, S. Hull, and D. Häusermann, *High Press. Res.* **8**, 625 (1992); M. Mezouar, Ph.D. thesis, Univ. Paris VII, 1997.
- ²⁴Y. LeGodec, D. Martinez-Garcia, M. Mezouar, G. Syfosse, J. P. Itié, and J. M. Besson, *High Press. Res.* **17**, 35 (2000).
- ²⁵J. Chomilier, G. Loupías and J. Felsteiner, *Nucl. Instrum. Methods Phys. Res. A* **235**, 603 (1985).
- ²⁶L. Marques, M. Mezouar, J.-L. Hodeau, and M. Nunez-Regueiro, *Phys. Rev. B* **65**, 100101 (2002); A. V. Talyzin, L. S. Dubrovinsky, M. Oden, T. Le Bihan, and U. Jansson, *ibid.* **66**, 165409 (2002).
- ²⁷T. Wagberg, P. Stenmark, and B. Sundqvist, *J. Phys. Chem. Solids* **65**, 317 (2004).
- ²⁸G. Oszlani, G. Baumgartner, G. Faigel, and L. Forro, *Phys. Rev. Lett.* **78**, 4438 (1997).
- ²⁹P. W. Stephens, G. Bortel, G. Faigel, M. Fegze, A. Janossy, S. Pekker, G. Oszlanyi, and L. Forro, *Nature (London)* **370**, 636 (1994).
- ³⁰Y. Kubozono, Y. Takabayashi, T. Kambe, S. Fujiki, S. Kashino, and S. Emura, *Phys. Rev. B* **63**, 045418 (2001).
- ³¹C. H. Choi, and M. Kertesz, *Chem. Phys. Lett.* **282**, 318 (1998).
- ³²C. Xu, C. Wang, C. Chan, and K. Ho, *J. Phys.: Condens. Matter* **4**, 6047 (1992).
- ³³S. C. Erwin, and C. Bruder, *Physica B* **199**, 600 (1994).
- ³⁴C. H. Kuntscher, G. M. Bendele, and P. W. Stephens *Phys. Rev. B* **55**, R3366 (1997).